BBA - Molecular and Cell Biology of Lipids 1862 (2017) 676–685

Contents lists available at ScienceDirect

BBA - Molecular and Cell Biology of Lipids

journal homepage: www.elsevier.com/locate/bbalip

Depletion of TM6SF2 disturbs membrane lipid composition and dynamics in HuH7 hepatoma cells

Hanna Ruhanen[a,b], P.A. Nidhina Haridas[a], Eeva-Liisa Eskelinen[b], Ove Eriksson[c], Vesa M. Olkkonen[a,d], Reijo Käkelä[b,*]

[a] Minerva Foundation Institute for Medical Research, Biomedicum 2U, FI-00290 Helsinki, Finland
[b] Department of Biosciences, University of Helsinki, FI-00014 Helsinki, Finland
[c] Biochemistry and Developmental Biology, Academic Medical Center Helsinki, Faculty of Medicine, University of Helsinki, FI-00014 Helsinki, Finland
[d] Department of Anatomy, Academic Medical Center Helsinki, Faculty of Medicine, University of Helsinki, FI-00014 Helsinki, Finland

ARTICLE INFO

Keywords:
Arachidonic acid
Fatty acid oxidation
Lipidome
Phosphatidylcholine
TM6SF2
Triacylglycerol

ABSTRACT

A polymorphism of *TM6SF2* associates with hepatic lipid accumulation and reduction of triacylglycerol (TAG) secretion, but the function of the encoded protein has remained enigmatic. We studied the effect of stable TM6SF2 knock-down on the lipid content and composition, mitochondrial fatty acid oxidation and organelle structure of HuH7 hepatoma cells. Knock-down of TM6SF2 resulted in intracellular accumulation of TAGs, cholesterol esters, phosphatidylcholine (PC) and phosphatidylethanolamine. In all of these lipid classes, polyunsaturated lipid species were significantly reduced while saturated and monounsaturated species increased their proportions. The PCs encountered relative and absolute arachidonic acid (AA, 20:4n-6) depletion, and AA was also reduced in the total cellular fatty acid pool. Synthesis and turnover of the hepatocellular glycerolipids was enhanced. The TM6SF2 knock-down cells secreted lipoprotein-like particles with a smaller diameter than in the controls, and more lysosome/endosome structures appeared in the knock-down cells. The mitochondrial capacity for palmitate oxidation was significantly reduced. These observations provide novel clues to TM6SF2 function and raise altered mebrane lipid composition and dynamics among the mechanism(s) by which the protein deficiency disturbs hepatic TAG secretion.

1. Introduction

Non-alcoholic fatty liver disease (NAFLD) with a global prevelance of 25 to 30% ranges from simple steatosis to non-alcoholic steatohepatitis (NASH) and cirrhosis, and can progress into hepatocellular carcinoma [1]. Genetic variants of patatin-like phospholipase domain containing 3, PNPLA3 (rs738409 and rs2281135), transmembrane 6 superfamily member 2, TM6SF2 (rs58542926) and membrane bound O-acyltransferase domain containing 7, MBOAT7 (rs641738) are associated with the development of NAFLD [2–4].

The allelic frequency of the *TM6SF2* variant is 7% and the carriers have increased susceptibility to NAFLD [3] but are protected from cardiovascular diseases [5]. *TM6SF2* is predominantly expressed in liver, small intestine and kidney. It encodes a protein of 351 amino acids with 7–10 predicted transmembrane domains. The variant *TM6SF2* encodes lysine instead of glutamine at position 167 of the protein (Glu167Lys). This substitution decreases the stability of the TM6SF2 protein [3]. TM6SF2 knock-down in mouse liver elevated the levels of hepatic cholesterol and triacylglycerols (TAGs), while very-low-density lipoprotein (VLDL) secretion was found to be reduced and the animals displayed reduced plasma cholesterol and TAG concentrations [3,5]. Consistently, hepatic TM6SF2 overexpression led to increased levels of hepatic total cholesterol and plasma low-density lipoprotein (LDL) cholesterol [6]. Recently, Smagris et al. [7] reported that the decrease of plasma TAGs in TM6SF2 knock-out mice is not due to reduced VLDL secretion but decreased lipidation of the VLDL particles.

The TM6SF2 protein is localized in the endoplasmic reticulum (ER) and the Golgi complex of hepatocytes [7,8], where the assembly and lipidation of VLDL particles takes place. Thus, the observed instability

Abbreviations: AA, arachidonic acid; ACC, acetyl-CoA carboxylase; CE, cholesterol ester; EM, electron microscopy; FA, fatty acid; MUFA, monounsaturated fatty acid; NAFLD, non-alcoholic fatty liver disease; NASH, non-alcoholic steatohepatitis; PC, phosphatidylcholine; PE, phosphatidylethanolamine; PI, phosphatidylinositol; PNPLA3, patatin-like phospholipase domain-containing protein 3; PUFA, polyunsaturated fatty acid; SFA, saturated fatty acid; shRNA, short hairpin RNA; TAG, triacylglycerol; TM6SF2, transmembrane 6 superfamily member 2

* Corresponding author at: Division of Physiology and Neuroscience, Department of Biosciences, University of Helsinki, Biocenter 3, P.O. Box 65, FI-00014 Helsinki, Finland.
E-mail address: reijo.kakela@helsinki.fi (R. Käkelä).

http://dx.doi.org/10.1016/j.bbalip.2017.04.004
Received 28 September 2016; Received in revised form 13 April 2017; Accepted 15 April 2017
Available online 18 April 2017
1388-1981/

of the variant TM6SF2 protein [3] may disturb the lipidation of VLDL particles. The membrane contents of polyunsaturated fatty acids (PUFAs), especially arachidonic acid (20:4n-6, AA), have recently been implicated in efficient clustering of TAGs for lipoprotein transport [9]. However, in TM6SF2 knock-out mice no major differences were found in the level of hepatic phosphatidylcholines (PCs) or in their fatty acid (FA) composition [7]. The knock-out mouse model of Fan et al. [6] rather implicated a predominant role of TM6SF2 in cholesterol metabolism. Thus, the mechanism of TM6SF2 function is unknown and the cause of increased hepatic lipid content in carriers of the variant allele is not understood.

In this study, we analyzed *in vitro* the effect of TM6SF2 on hepatocyte lipid content and lipid species composition using the human hepatocyte cell line HuH7 subjected to knock-down of TM6SF2. Pulse chase experiments with [^{13}C]glycerol were performed to investigate the turnover rates of different lipids. To investigate the functional consequences of the lipid alterations, we studied the rates of mitochondrial oxygen consumption (OCR) with FA as substrate, in the control and TM6SF2 knock-down cells. In addition, electron and fluorescence microscopy were employed to observe possible differences in organelle structure or distribution between the TM6SF2 deficient and control cells. The hallmark observations in the TM6SF2 knock-down cells were an enrichment of saturated (SFAs) and monounsaturated FAs (MUFAs) in storage and membrane lipids, a depletion of AA in PCs, and functional changes indicated by a reduced mitochondrial OCR with FA as substrate, an increase in the number of lysosome/endosome structures as compared to controls, and reduced size of secreted lipoprotein-like particles. These observations provide novel clues to the TM6SF2 function and suggest that an altered membrane lipid composition and dynamics play roles in the mechanism(s) by which the protein deficiency disturbs hepatic TAG secretion.

2. Materials and methods

2.1. Cell culture and generation of HuH7 hepatocytes with TM6SF2 stably knocked down

TM6SF2 knock-down HuH7 hepatocytes were generated using a lentiviral transduction approach. Briefly, HuH7 cells were cultured in MEM AQ™ (Minimal essential Eagle medium; Sigma-Aldrich, St. Louis, MO) with 10% FBS (fetal bovine serum), 100 μg/ml streptomycin and 100 U/ml penicillin. Cells were grown to 70% confluency and transduced with lentiviral particles encoding shRNA against TM6SF2 (TRCN0000254085, Sigma-Aldrich) or a non-targeting control (SHC002V), according to the manufacturer's protocol. Transduced cells were selected with puromycin (5 μg/ml). The selected cells were grown further in the above medium containing puromycin and used for further experiments. The experiments were performed using two independent biological replicates.

2.2. Gene expression analysis (qPCR)

Expression of *TM6SF2* gene was analyzed by quantitative polymerase chain reaction (qPCR) by using Light Cycler 480 II (Roche Applied Science, Penzberg, Germany). Total RNA was extracted from the TM6SF2 knock-down and control HuH7 cells using PureLink® RNA Mini Kit according to the manufacturer's protocol. cDNA synthesis was carried out using SuperScript® VILO™ reverse transcriptase kit (Invitrogen, Carlsbad, CA). Quantitative real time PCR was performed with gene-specific primers (Table S1) and Roche SYBR-Green® master mix. SDHA (Succinate dehydrogenase complex, subunit A) and β-actin were used as housekeeping references, and the data were normalized to a geometric mean of these.

2.3. Lipid labeling and analysis by mass spectrometry and gas chromatography

For lipidomics, HuH7 cells cultured on 6-well plates as specified above were washed with PBS and scraped into 1 ml of ice-cold 0.25 M sucrose. For analysis of lipid turnover, the medium of the cells on 6-well plates was on the day one after plating changed to a labeling medium containing 500 μg/ml of [^{13}C]glycerol (Cambridge Isotope Laboratories, Andover, MA). The cells were first incubated for 24 h and then chased for another 24 h in medium containing 5 mg/ml of unlabeled glycerol.

Cellular lipids were extracted according to Folch et al. [10] and dissolved in chloroform/methanol 1:2 (by vol). Just before mass spectrometry, 1% NH_4OH was added along with a cocktail of internal lipid standards containing respresentatives for all lipid classes analyzed. The samples were injected into the electrospray source of a triple quadrupole mass spectrometer (Agilent 6490 Triple Quad LC/MS with iFunnel Technology; Agilent Technologies, Santa Clara, CA) at a flow rate of 10 μl/min, and spectra were recorded using both positive and negative ionization mode. TAGs were detected as $(M + NH_4)^+$ ions [11] and cholesterol esters (CEs) using precursor ion scanning of *m/z* 369 (P369) in the positive ion mode [12]. Phospholipid species were selectively detected using head-group specific MS/MS scanning modes (PC: P184, PE: neutral loss of 141 (NL141), PI: P241) [13]. The unlabeled [M] and [^{13}C]glycerol-labeled [M + 3] ions were resolved by comparing the spectra of cell samples with or without labeling, and deconvolution into different species was performed by the best profile fitting available in LIMSA software [14]. FA composition of total lipids was determined by gas chromatography (quantitation by Shimadzu GC-2010 Plus equipment with flame-ionization detector, GC-FID, and identification of FA structures by Shimadzu GCMSQP2010 Ultra with mass selective detector, GC-MSD) using procedures detailed in Käkelä et al. [15]. In order to confirm the glycerolipid acyl chain assembly, precursor scans for the main acyl chains, first detected by GC, were recorded by ESI-MS/MS using negative mode precursor scans for the acyl fragments released from PEs and PC formate adducts. The acyl chains of the TAGs were verified by positive mode ESI-MS/MS using acyl chain specific NL scans. Mass spectra were processed by MassHunter software (Agilent Technologies, Inc. California, USA) and individual lipid species were quantified using the internal standards and LIMSA software.

2.4. Analysis of de novo lipogenesis

HuH7 control and TM6SF2 knock-down cells were grown on 6-well plates to confluency. Cells were then incubated with [^{3}H]-Acetic acid (150 μCi/well; Amersham, GE Healthcare) in complete media for 3 h. Cells were washed and scraped in 2% sodium chloride. Total lipids were extracted according to Bligh and Dyer [16]. The samples were run on thin layer silica based chromatography using hexane/diethyl ether/acetic acid/H_2O (65:15:1:0.25,vol/vol) as the solvent system. TAG and CE standards were run on TLC along with the samples to identify the corresponding species. TAG and CE bands were scraped, the [^{3}H] radioactivity was measured by liquid scintillation counting, and the results normalized for total cell protein.

2.5. Glucose uptake assay

Glucose uptake assay was done in HuH7 control and TM6SF2 knock-down cells, which were starved in serum free, glucose free DMEM (A14430-01, Thermo Scientific) for one hour, after which glucose uptake was initiated by the addition of 0.5 ml DMEM with 100 μM cold D-glucose and 0.1 μCi of deoxy-D-glucose 2-[1,2-^{3}H (N)] (Perkin Elmer). The uptake was terminated by removing the media and adding ice cold PBS. The cells were washed and then lysed with 0.1% sodium dodecyl sulfate (SDS). The radioactivity in the cells was measured by

liquid scintillation counting. The radioactive counts were normalized to total protein.

2.6. Glycogen synthesis assay

HuH7 control and TM6SF2 knock-down cells were grown on 6-well plates to confluency. The cells were starved overnight in DMEM (D5546, Sigma-Aldrich) containing 0.5% BSA and 2 mM L-glutamine. Next day the cells were incubated in 0.18 μCi/μmol D- [U-^{14}C]-glucose (PerkinElmer) for 1 or 4 h, washed with ice cold PBS and frozen overnight in − 20 °C. Samples were lysed in 0.7 ml 0.03% SDS and 0.4 ml of the suspension was transferred to 2 ml tubes together with 1 mg carrier glycogen. The remaining cell suspension was used for protein concentration determination by the bicinchoninic acid (BCA) assay (Thermo Scientific, Waltham, MA). The original samples were heated in 100 °C for 30 min. Glycogen was precipitated by addition of 99% ethanol and incubated overnight in − 20 °C. Glycogen pellets were collected by centrifugation for 15 min at 10000 rpm, washed once with 70% ethanol and resuspended in 200 ml distilled water. Radioactivity was determined by liquid scintillation counting. Each experiment was carried out on triplicate wells.

2.7. Analysis of mitocondrial oxygen consumption rate (OCR)

The OCR of control and TM6SF2 knock-down cells was measured using the Seahorse XF96 Extracellular Flux Analyzer (Agilent Technologies). Both control and TM6SF2 knock-down HuH7 cells were plated onto Poly-L-Lysine coated XF96 cell culture micro plates (Agilent Technologies). Cells were grown until confluency in growth medium, followed by a serum starvation for 4 h in XF base medium (Agilent Technologies) supplemented with 0.5 mM glucose, 1 mM glutamine and 0.5 mM carnitine. Cells were then moved to a CO_2 free incubator and incubated for another 1 h in XF base medium supplemented with 0.5 mM glucose and 0.5 mM carnitine, after which cells were treated with 0.17 mM FA free BSA or 0.16 mM palmitic acid (Sigma–Aldrich) conjugated with FA free BSA, and incubated for an additional 1 h. The OCR was measured using the XF Cell Mito Stress Test Kit (Agilent Technologies) with following additions: oligomycin (0.6 μM), FCCP (0.5 μM), and rotenone (0.5 μM) plus antimycin A (0.5 μM). Three 3-min cycles were measured for each condition and the OCR were normalized to total protein content of each well determined by the BCA assay. The basal respiration due to utilization of exogenous FAs was calculated according to the manufacturer's protocol (basal palmitate-BSA rate minus basal BSA rate minus OCR due to uncoupling by free FAs).

2.8. Electron microscopy (EM) of cells

The cells were grown on glass cover slips for flat embedding, while normal cell culture dishes were used for pellet embedding. For flat embedding, the cells were fixed in 2% glutaraldehyde in 0.1 M cacodylate buffer, pH 7.4, for 30 min at room temperature. For pelleting, cells were fixed in 2% glutaraldehyde in 0.2 M Hepes, pH 7.4, at room temperature for 2 h. The cells were then scraped off the dish after 30-min fixation, pelleted with a microcentrifuge in the fixative, and the fixation was continued as a pellet. The fixed cells and cell pellets were then washed, post-fixed in 1% osmium tetroxide, dehydrated in ethanol and acetone, and embedded in TAAB resin. Thin sections were cut using a diamond knife and stained with uranyl acetate and lead citrate.

Pelleted cells were used for quantification of cytoplasmic volume fractions due to the random orientation of cells in relation to the section plane in such specimens. Micrographs were taken using uniform random sampling at 2000 × primary magnification, using a Jeol JEM-1400 transmission electron microscope. A total of 65–70 micrographs for each sample were used for the quantification. The area of the cytoplasm and the organelles was quantified using point counting as detailed in [17]. The ratio of the organelle area per cytoplasmic area was used as an estimate for the volume fraction.

2.9. Immunofluorescence microscopy

TM6SF2 knock-down and control HuH7 cells on coverslips were fixed with 4% paraformaldehyde in PBS and permeabilised using 0.1% Triton X-100. Cells were then washed twice with PBS and unspecific antibody binding was blocked with 10% FBS, followed by incubation with anti-LAMP1 (H4A3, Santa Cruz biotechnology) for 2 h at room temperature. Cells were then washed thrice using PBS and incubated with Alexa Fluor®488- Anti-mouse (A11001, Invitrogen Life Sciences). After washing thrice the coverslips were mounted using Mowiol (Calbiochem, La Jolla, CA) containing 50 mg/ml 1,4-Diazabicyclo-[2.2.2] octane (Sigma–Aldrich) and 5 μg/ml DAPI (Thermo Scientific/Molecular Probes). Cells were imaged using Zeiss Axio Observer Z1 microscope (Carl Zeiss Imaging Solutions GmbH, Oberkochen, Germany) with an objective of 63 × magnification and numerical aperture 1.4 and Colibri laser and with same exposure time for both control and knock-down cells. LAMP1 stainings were quantified using FIJI (Image J) software with a set cutoff threshold (total signal intensity/number of cells in the field). Approximately 100 cells were measured in both TM6SF2 knock-down and control specimens.

2.10. EM of secreted lipoprotein-like particles

HuH7 control and TM6SF2 knock-down cells were grown in 75 cm^3 flasks to confluency, after which media samples were collected and concentrated using Spectra/Por® 4 dialysis tubing (Spectrum Laboratories, Inc., California, USA) against crystal sucrose and then dialyzed against PBS. The samples were centrifuged, pipetted on formwar-coated, glow discharged grids and negative stained using 1% phosphotungstic acid. Micrographs were taken using a Jeol JEM-1400 transmission electron microscope. Electron micrographs were processed using ImageJ open platform image processing program to analyze secreted particles. A median filter was first applied using a kernel of a radius of 5-pixels, then the images were automatically thresholded using the percentile method. Thresholded images were used to detect regions with an area between 1000 and 3000 pixels square and a circularity value of at least 0.3. This method allowed reliable automated detection of secreted particles within the defined range. The Pixel value was converted to nm^2 and the diameter of the particles were calculated.

2.11. Quantification of apolipoprotein B100 secretion

HuH7 control and TM6SF2 knock-down cells grown on 12-well plates were kept overnight in MEM AQ™ containing 100 μg/ml streptomycin and 100 U/ml penicillin, and the following day the media were collected, centrifuged and stored at − 20 °C. The cells were lysed and used for protein concentration determination by the BCA assay. The media were analyzed using Human Apolipoprotein B ELISA^{PRO} kit (3715-1HP-2, Mabtech, Sweden) according to the manufacturer's protocol. The absorbance was measured at 450 nm in a microplate reader and a 4-parameter curve fitting program was used for data analysis.

2.12. Statistical analysis

For univariate comparisons statistical significance was determined by a two-tailed Student's *t*-test. For multivariate comparisons of detailed lipid profiles, Principal Component Analysis (PCA) (Sirius, PRS, Bergen, Norway) was used. The PCA shows compositional differences between the samples, and highlights the lipid species mainly responsible for the variation in the data. For PCA, arcsine transformed data were used and the relative positions of the samples and variables were plotted using the first two principal components. The differences between the groups seen in the PCA were further quantitatively analyzed using Soft

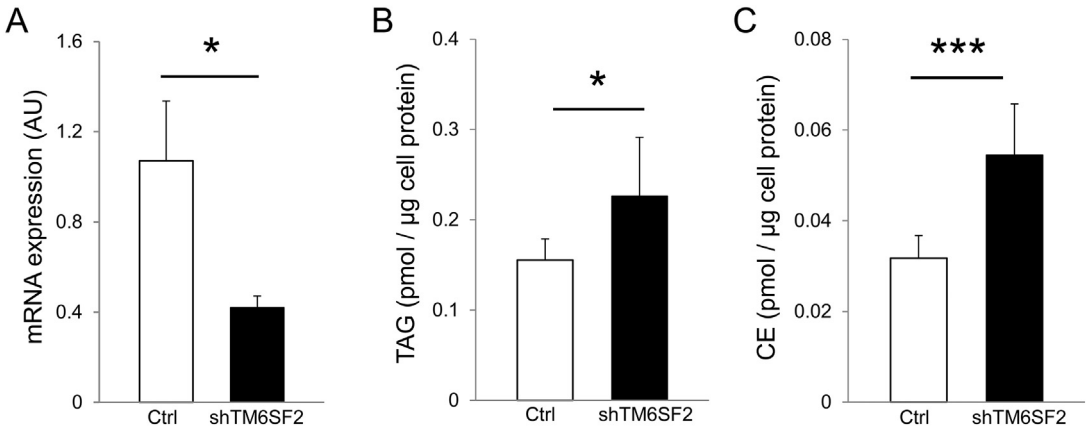

Fig. 1. Knocking down TM6SF2 increases TAG and CE levels in HuH7 cells. (A) TM6SF2 mRNA expression levels analyzed by qPCR. TM6SF2 was stably knocked down using lentiviral particles encoding shRNA against TM6SF2 (shTM6SF2); control (Ctrl) cells were transduced with a non-targeting shRNA encoding virus ($n = 3$). (B-C) Total quantity of TAGs and CEs after 24-h culture, analyzed by ESI-MS/MS. The values represent mean ± SD ($n = 6$); * $p < 0.05$, *** $p < 0.001$.

Independent Modeling of Class Analogy (SIMCA; Sirius) [18].

3. Results

3.1. Triacylglycerol and cholesterol ester concentrations are increased in HuH7 hepatocytes with TM6SF2 stably knocked down

HuH7 cells were subjected to stable knock-down of TM6SF2 using a shRNA expressing lentivirus. To avoid biases caused by phenotypic aberrations frequently occurring in single-cell clones, pools of transduced cells were analyzed. In such pools, an average knock-down efficiency of 60% at the mRNA level was observed as compared to controls transduced with a non-targeting shRNA lentivirus (Fig. 1A). Upon mass spectrometric analysis of the cellular lipids, significant elevations of total TAG (32%) and CE (41%) concentrations were observed in the TM6SF2 knock-down cells (Fig. 1B–C), consistent with previously published reports [3,8].

3.2. TM6SF2 silenced cells are relatively depleted of PUFA containing lipids and enriched in SFA and MUFA containing lipids

Lipid species profiles of the control and TM6SF2 knock-down cells were subjected to PCA to reveal lipidome differences between the cell pools (Fig. 2A–D) (The full lipid species data are shown in Tables S2–6). The most important principal component PC1 (horizontal axes) represented the degree of unsaturation of the lipid species, and explained 60% (TAG), 64% (CE), 88% (PC) or 93% (PE) of the variation in the lipid classes displayed (Fig. 2A–D). When focusing on TAG composition, the control cells grouped on the left-hand side of the PCA biplot *i.e.* they contained more TAGs with PUFA moieties (*e.g.* TAG species 56:6, 56:7, 58:7, and 58:8) whereas the TM6SF2 knock-down cells grouped on the right-hand side, and were characterized by TAGs with SFAs and MUFAs (Fig. 2A). The difference in the TAG species profiles of the control and TM6SF2 knock-down was significant according to SIMCA ($p < 0.05$).

When CE species were used as loadings, PCA indicated a similar loss of unsaturated acyl chains in TM6SF2 knock-down cells as was found for the TAGs (Fig. 2B). The most divergent CE species variable, located furthest from the origin, was CE 22:6 (CE with docosahexaenoic acid, or DHA, moiety). In general, TM6SF2 knock-down cells (5 out of 6 replicates) contained smaller relative amounts of CE 22:6 and at the same time more of SFA and MUFA containing CEs as compared to the controls.

For the major membrane phospholipids of the cells, PCs and PEs, the PCA separation by PC1 (acyl chain unsaturation) was very clear (Fig. 2C–D) and quantitatively significant (SIMCA, $p < 0.05$). Of note, this change in the PC and PE species composition was accompanied by an increase in the total level of cellular PCs and PEs in the TM6SF2 knock-down cells as compared to controls (inserts, Fig. 2C–D). Similar to the TAGs and CEs, the TM6SF2 knock-down cells contained higher relative amounts of PC and PE species carrying SFAs and MUFAs and less species with PUFA chains, especially AA (*e.g.* 36:4, 38:4, and 38:5, the presence of AA verified upon fragmentation by ESI-MS/MS). This suggests that there is a global shift in the lipid species profile of the TM6SF2 knock-down cells. Furthermore, when the FA composition in the total lipids of the cells after 24 h culture was investigated by gas chromatography, the total level of AA was found to be significantly lower ($p < 0.01$) in the TM6SF2 knock-down cells as compared to controls (Table S7).

3.3. Absolute levels of AA containing PCs are decreased in TM6SF2 knock-down cells

In order to clarify whether the changes observed in the phospholipid species composition of the TM6SF2 knock-down cells were due to increase in the levels of SFA/MUFAs containing species or decrease of PUFA (especially AA) containing species, or possibly both, we calculated the absolute levels of these lipids by normalizing them to total cellular protein. In PCs, but not in any other phospholipid class analyzed (PEs and PIs), the absolute levels of AA containing species 36:4 and 38:5 were in 24-h cultures significantly lower in TM6SF2 knock-down cells as compared to controls (Fig. 3A). After extended (one week) culture time also the difference in PC 38:4 became significant (Fig. 3B). When looking at the levels of SFA/MUFA containing lipids, significant increases in the absolute levels of PC 34:2, 36:1 and 36:2 at the 24-h time point and PC 34:1, 36:1 and 36:2 at the one week time point were observed in the TM6SF2 knock-down cells as compared to controls (Fig. 3A–B). Comparison of the 24-h and one week culture times revealed that, overall, the differences in the lipid levels between the cell pools became more pronounced over the time.

3.4. Glycerolipid turnover is enhanced in TM6SF2 knock-down cells

[^{13}C]glycerol labeling was employed to study the synthesis and turnover of glycerolipids in the TM6SF2 knock-down cell model. Significantly higher total levels of [^{13}C]glycerol labeled TAGs, PCs, PEs, and PIs accumulated in the TM6SF2 knock-down cells as compared to controls during 24 h (Fig. 4A–D). However, during 24-h chase in a medium containing unlabeled glycerol, the amount of the labeled lipids also reduced more rapidly in the TM6SF2 knock-down cells as compared to controls (turnover rates are indicated by the slopes visualized in the panels of Fig. 4). Consistent with the enhanced incorporation of [^{13}C]glycerol into TAGs, we also observed an elevation

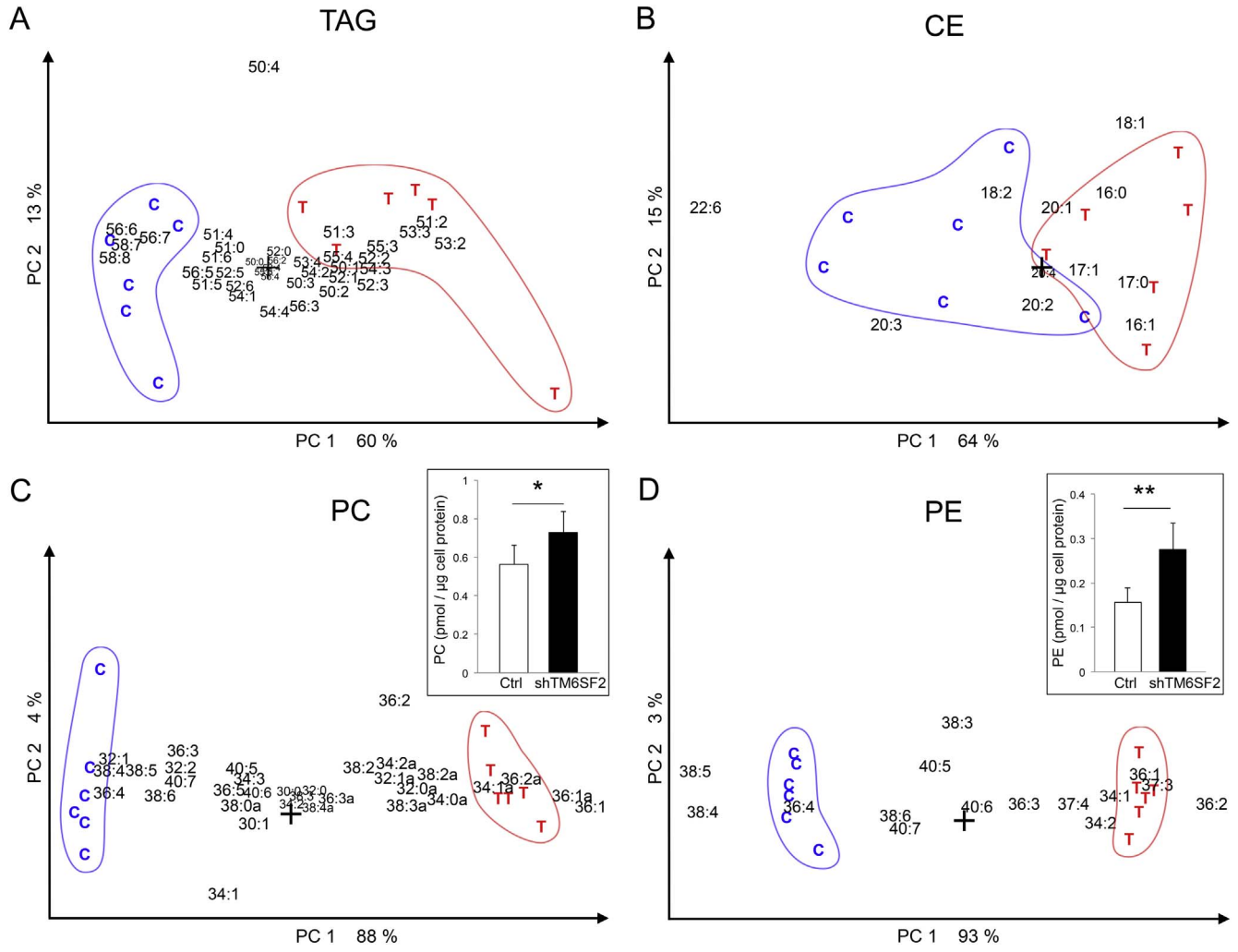

Fig. 2. Principal component analysis (PCA) of the effect of TM6SF2 knock-down on the lipid profile of HuH7 cells. TM6SF2 knock-down and control cells were cultured for 24 h, the lipid species analyzed as described in Material and Methods, and the data subjected to PCA. The samples located furthest from the origin of the PCA biplot (marked as +) on one side contain relatively more of the lipid species furthest on that same side. The longer the distance between two samples on the plot the more their lipid profiles differ from each other. Arrows show the direction of the Principal Components 1 and 2 (PC1 and PC2) and the percentages represent the proportion of the variation in the data each PC axis explains. (A) PCA of TAG species. Lipid species present at > 0.5% were used as variables. The species are identified as 'number of carbons':'number of double bonds' in the acyl chains. C, control; T, shTM6SF2. (B) PCA of CEs. All analyzed species were used as variables. (C) PCA of PCs. Species present at > 0.5% were used as variables. a = alkyl-acyl species. (D) PCA of PEs. All analyzed lipids were used as variables. Total quantities of PCs and PEs are shown in the inserts. Values in the inserts represent mean ± SD ($n = 6$); * $p < 0.05$, ** $p < 0.01$.

of [^3H]acetic acid incorporation into TAGs and CEs during a 3-h labeling, as a measure of *de novo* lipogenesis (Fig. S1). However, glucose uptake or glycogen synthesis were not affected (Fig. S2).

3.5. TM6SF2 knock-down cells secrete smaller lipoprotein-like particles

We next wanted to see if changes in the lipid profile of the cells associate with an altered secretion of lipoproteins. We performed EM of particles secreted into growth media of control and TM6SF2 knock-down cells. While large, spherical lipoprotein-like particles were prominently present in the medium of control cells, the size of the particles secreted by TM6SF2 knock-down cells was markedly smaller (Fig. 5A). The relative particle size distribution of the cells (Fig. 5B) revealed that particles > 20 nm in diameter were nearly undetectable in the medium of TM6SF2 knock-down cells. However, apolipoprotein B100 secretion was not reduced but rather slightly increased in the TM6SF2 knock-down cells (Fig. 5C).

3.6. TM6SF2 knock-down cells display a reduced rate of mitochondrial fatty acid oxidation

Mitochondrial β-oxidation was measured by the mitochondrial oxygen consumption rate (OCR) in TM6SF2 knock-down and control cells, using palmitic acid (16:0) as substrate. The result of a mitochondrial stress test experiment carried out with the Seahorse® metabolic flux analyzer is presented in Fig. 6. The measurements showed that the basal OCR in the presence of palmitic acid was higher in control cells than in the TM6SF2 knock-down cells (Fig. 6A–B). Both TM6SF2 knock-down and control cells responded to the addition of the ATP-synthase inhibitor oligomycin by a decrease in the OCR (Fig. 6A). Subsequent addition of the uncoupler FCCP lead to a rapid activation of the OCR in both TM6SF2 knock-down and control cells (Fig. 6A). These finding indicate that TM6SF2 knock-down lead to a decreased basal OCR, while the mechanisms coupling ATP production to oxygen consumption remained unaffected, suggesting that TM6SF2 knock-down selectively acted on some component(s) required for β-oxidation. Quantitative analysis yielded that TM6SF2 knock-down lead to a 63% drop in the basal palmitate-driven OCR, compared to control cells (Fig. 6B).

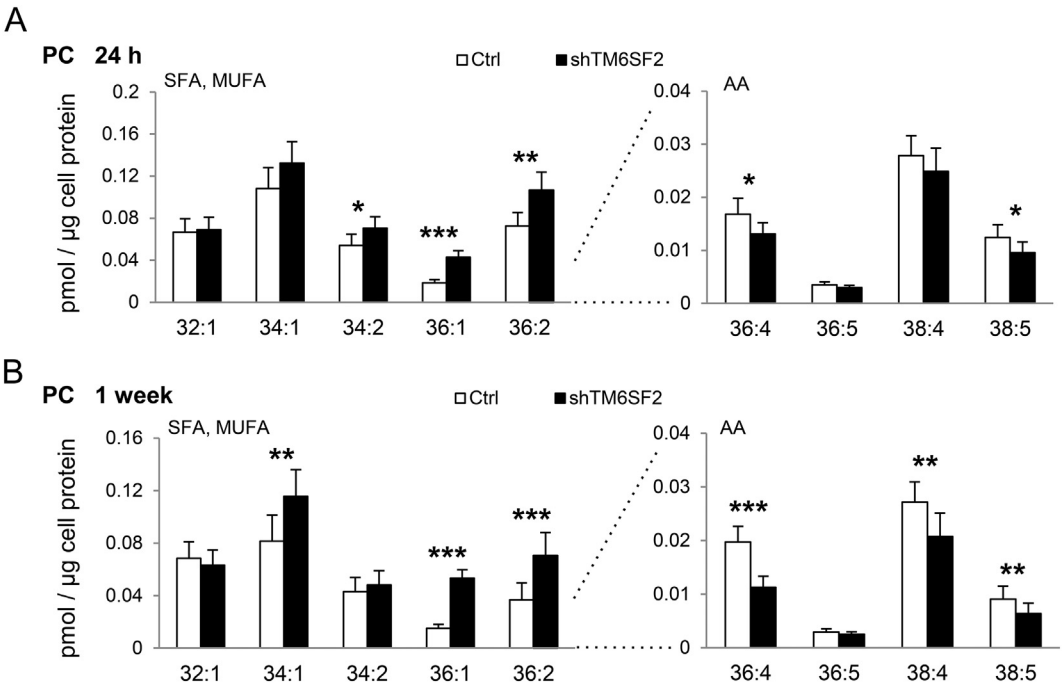

Fig. 3. Knocking down TM6SF2 increases levels of PCs with SFA and MUFA moieties and decreases levels of AA (20:4n-6)-containing PCs. Quantities of the major PC species with SFA, MUFA and AA moieties analyzed by ESI-MS/MS after culturing the cells for 24 h (A) or one week (B) are shown. The values represent mean ± SD ($n = 6$); * $p < 0.05$, ** $p < 0.01$, *** $p < 0.001$.

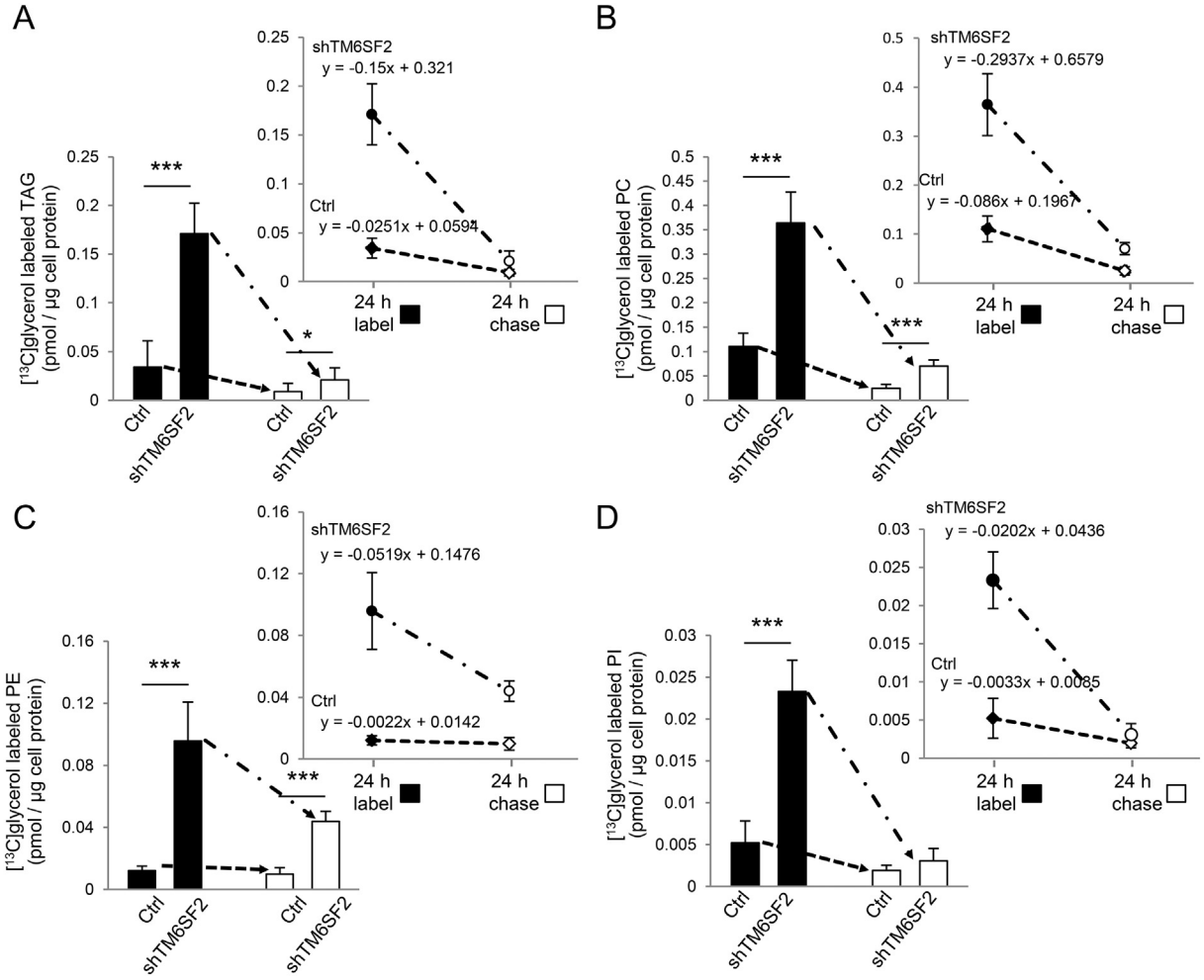

Fig. 4. Glycerolipid turnover is enhanced in TM6SF2 knock-down hepatocytes. Total quantity of [^{13}C]glycerol labeled TAGs (A), PCs (B), PEs (C) and PIs (D) after 24-h labeling and 24-h chase, analyzed by ESI-MS/MS, are shown. Turnover rates are indicated by the slopes in the panels. The values represent mean ± SD ($n = 6$); *** $p < 0.001$.

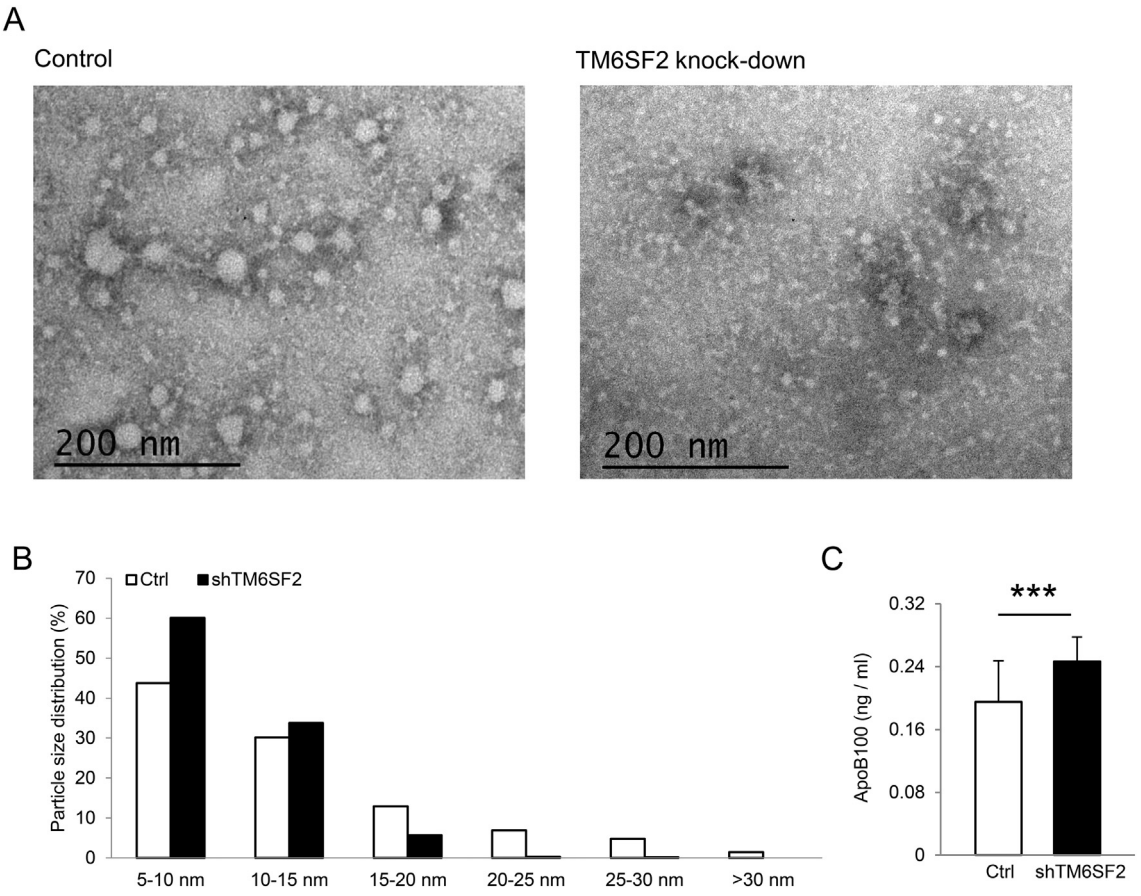

Fig. 5. TM6SF2 knock-down hepatocytes secrete smaller lipoprotein-like particles into growth medium. (A) Electron microscopy images of secreted particles after negative staining of the media samples. (B) Relative size distribution of the secreted particles (the number of quantified particles: Ctrl, 813; shTM6SF2, 651). (C) Apolipoprotein B100 secretion measured by ELISA and normalized for total cellular protein. The values represent mean ± SD (n = 17); *** $p < 0.001$.

3.7. Expansion of late endosome/lysosome structures in TM6SF2 knock-down hepatocytes

A significant increase in the absolute cellular concentrations (per total cell protein) of the major classes of membrane phospholipids, PCs and PEs, was observed in the TM6SF2 knock-down hepatocytes (see Fig. 2C–D). We therefore carried out EM in order to detect possible differences in organelle structure of the cells. An increased number of late endosomes/lysosomes was evident in the sections of TM6SF2 knock-down cells as compared to controls. Quantification of the volume fraction of late endosomes/lysosomes in the cytoplasmic compartment of these cells revealed a 2.9-fold increase relative to the controls (Fig. 7A). To further confirm this observation, we performed immunofluorescence microscopy with antibodies against the lysosome marker LAMP1. The LAMP1 staining intensity was 2-fold higher in the TM6SF2 knock-down cells than in the controls (Fig. 7B), consistent with an

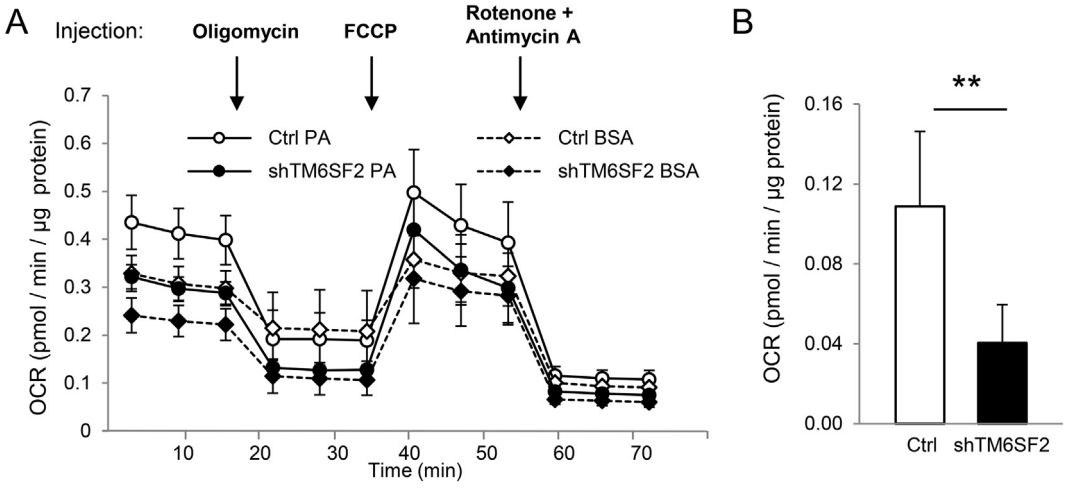

Fig. 6. Oxygen consumption rate (OCR) in the presence of palmitic acid is reduced in TM6SF2 knock-down hepatocytes. ORC was measured in real-time using the Seahorse® metabolic flux analyzer as described in Materials and Methods. (A) The OCR curves; the times of addition of oligomycin, FCCP, and rotenone + antimycin A are indicated at the top. OCR in the presence of palmitate-BSA (PA) and BSA are displayed. (B) Basal OCR due to utilization of exogenous fatty acids. The values represent mean ± SD (n = 7–10); ** $p < 0.01$.

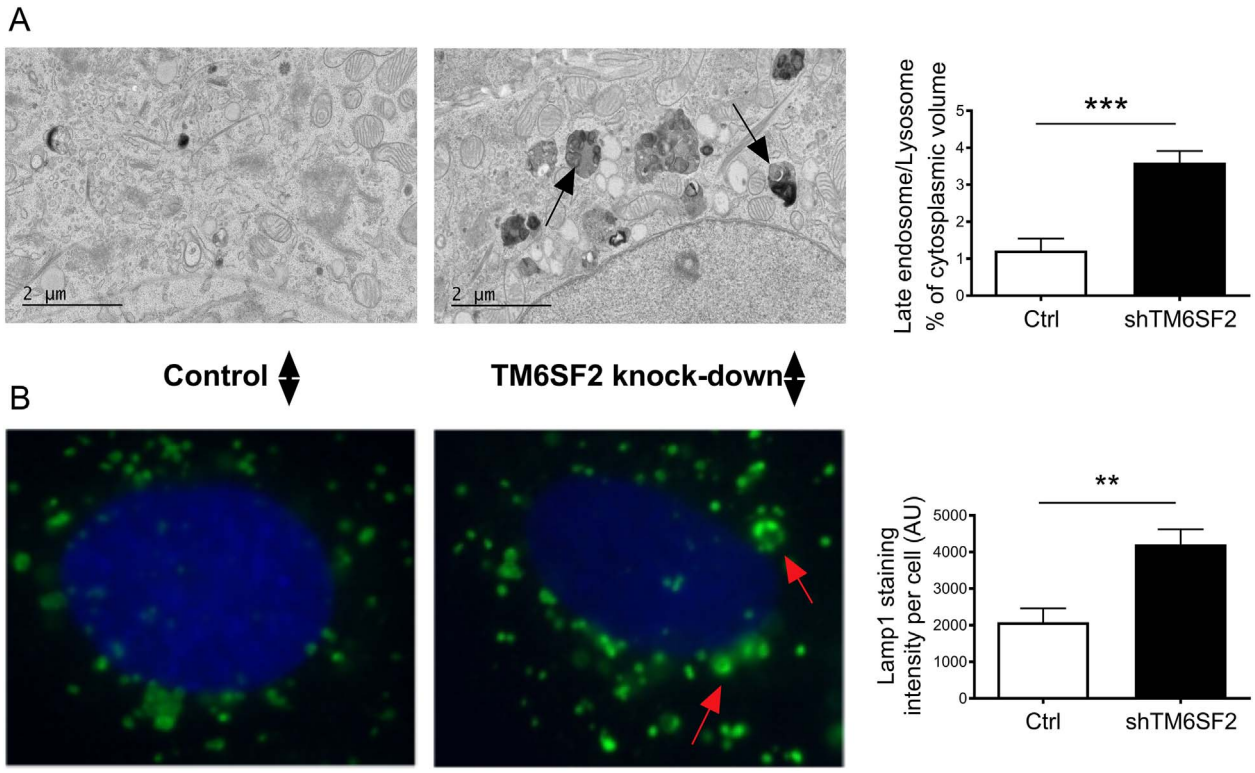

Fig. 7. Amplification of late endosome/lysosome structures in TM6SF2 knock-down hepatocytes. (A) Electron microscopy images showing more lysosome/late endosome structures in TM6SF2 knock-down cells (shTM6SF2) as compared to controls. The quantifications represented are from 60 to 70 micrographs. (B) Lamp1 staining of control and TM6SF2 knock-down cells and its quantification (from 100 to 120 cells). The values represent mean ± SEM, ** $p < 0.01$, *** $p < 0.001$.

amplification of the late endosomal/lysosomal compartments.

4. Discussion

TM6SF2 is a novel key regulator of hepatic VLDL TAG secretion. Its common sequence variant reducing the stability of the encoded protein [3] associates with hepatic TAG accumulation but acts protective against cardiovascular diseases [5,19]. However, the molecular mechanisms of TM6SF2 function have remained enigmatic. In the present study we knocked down TM6SF2 by 60% in the human HuH7 hepatoma cell line, which has been employed in previous investigations as a hepatocyte model to assess the function of TM6SF2 [3,8]. Mass spectrometric analysis of the cellular lipidome and its dynamics, measurements of mitochondrial oxygen consumption rate and studies of organelle structure revealed that TM6SF2 knock-down results in (i) Accumulation of TAGs and CEs in the cells, (ii) Relative enrichment of SFAs/MUFAs in all major lipid classes, (iii) Absolute increase of PCs and PEs with SFAs and MUFAs, (iv) Relative and absolute depletion of AA from PCs, (v) Enhanced synthesis and turnover of the hepatocellular membrane and storage lipids, (vi) Modification of the total cellular FA pool, with SFAs/MUFAs increased and AA reduced, (vii) Reduction in the size of secreted lipoprotein-like particles, (viii) Defect in mitochondrial OCR in the presence of a FA substrate, and finally (ix) Increase of the volume of late endosomal/lysosomal compartments. Depletion of TM6SF2 thus has extensive, global effects on hepatocellular lipid metabolism.

It is becoming evident that the hepatic lipid composition plays a major role in lipoprotein secretion, lipid accumulation and pathology. The excess SFAs and MUFAs found in this work in the TM6SF2 knock-down cells, have been reported to have deleterious effects on liver function and cause tissue damage [20]. In our cell model, the accumulation of SFAs and MUFAs could be due to the elevated *de novo* lipogenesis utilizing these acyl chains, or occur through other mechanisms such as enhanced SCD1 activity in the knock-down cells. Stearoyl desaturase 1 (SCD1, Δ-9 desaturase) activity was found to increase in fatty liver diseases, leading to the accumulation of MUFAs [21], and inhibition of SCD1 reduced the induction of hepatic steatosis in mouse models [22]. On the other hand, increased SCD1 activity was also suggested to have a protective effect against hepatic injury. SCD1 converts SFAs to MUFAs, enhances the incorporation of MUFAs to TAGs, and protects the liver from the lipotoxicity of SFAs [23]. Similar to the TM6SF2 knock-down cells, the hepatic PUFA levels of NASH patients were found to be low and the degree of PUFA reduction was reported to correlate with disease severity [24]. In addition, a variant of FA desaturase 1 (FADS1, Δ-5 desaturase), impairing the insertion of the last double bond when producing AA, has been associated with hepatic lipid accumulation [25]. Moreover, cells and mice deficient in lysophosphatidylcholine acyltransferase 3 (LPCAT3) had reduced levels of AA in their membrane phospholipids, PCs in particular, resulting in defective lipoprotein secretion [9,26]. Thus aberrations of different proteins modifying or transferring FAs may drive the hepatic lipid accumulation.

The hepatocyte TM6SF2 protein has been localized to the ER and the Golgi apparatus [7,8], key organelles of the secretory pathway responsible for the assembly and secretion of VLDL [27,28]. It is thus plausible that this gene product may modify the lipid composition of the secretory pathway membranes in a manner that promotes their compatibility with lipoprotein production. Thus the reduction of PCs with AA in our TM6SF2 knock-down cells is an especially interesting finding and may represent a key to the observed cellular neutral lipid accumulation. In mice, a similar reduction of AA in membrane phospholipids due to LPCAT3 deficiency caused a marked reduction of plasma VLDL-TAGs with concomitant hepatic steatosis [26], a phenotype reminiscent of that observed in TM6SF2 knock-out mice [7]. Consistent with the study of Smagris et al. [7], we also observed a reduction in the size distribution of lipoprotein-like particles secreted by the TM6SF2 knock-down cells, while production of apoB100 was not defective.

Besides impaired lipoprotein secretion, the increased lipid content of liver tissue or cultured hepatocytes upon TM6SF2 knock-down or knock-out [3,5,7,8] may in principle reflect enhanced hepatic FA uptake or *de novo* lipogenesis, reduced mitochondrial oxidation of FAs, or a defect of glucose metabolism and storage as glycogen. We observed in the TM6SF2 knock-down hepatocytes enhanced *de novo* lipogenesis and reduced FA oxidation. However, no significant alteration of glucose uptake or glycogen synthesis was detected (Fig. S2), pointing to a primary function of TM6SF2 in lipid metabolism. Labeling/chase of lipids with [^{13}C]glycerol revealed both enhanced lipid synthesis and turnover in the TM6SF2 knock-down cells. If the balance of these counteracting homeostatic distortions is biased towards increased synthesis, as indicated by the enhanced *de novo* lipogenesis observed, this could be one plausible cause of the lipid accumulation observed in the TM6SF2 depleted cells. On the other hand, the fact that also the lipid turnover was increased in the TM6SF2 knock-down cells may explain why the TAG accumulation in our model was not dramatic. The reason for the enhanced dynamics of lipid synthesis/turnover is so far unknown. One possible mechanistic explanation to the increased *de novo* lipogenesis is ER stress caused by TAG accumulation. TM6SF2 deficiency has been reported to result in ER stress [29], which is known to induce several signaling pathways upregulating hepatic lipogenesis [30]. One is also tempted to speculate that a distortion of the FA composition of phospholipids (*i.e.* reduction of PUFAs, AA in particular), may trigger a futile cellular response aimed at maintaining an optimal composition of membrane lipids *via* enhanced phospholipid synthesis, at the end manifested in the excess of storage lipids as well. In addition to TM6SF2, deficient variants of PNPLA3, MBOAT7 and MBOAT5, which recently were implicated in acyl-chain remodeling of lipids, also induce fatty liver [26,31,32]. Thus, a possible role of TM6SF2 in incorporating AA and other PUFAs into membrane phospholipids should be studied further.

Impaired FA oxidation and ultrastructural changes in mitochondria have been reported as causes of mitochondrial dysfunction in NAFLD [33,34]. Therefore, we considered mitochondrial dysfunction as one tentative reason for the lipid accumulation in the TM6SF2 silenced cells. The present observations indeed suggest impaired mitochondrial FA oxidation in these cells. Thus, besides defective TAG secretion and a tentative dysbalance in lipid synthesis/turnover, reduced mitochondrial FA oxidation may be a putative cause of the cellular accumulation of TAGs, CEs, PCs and PEs in the present cell model. Of note, only hepatic TAG and CE but not phospholipid accumulation was previously detected in the TM6SF2 knock-out mice [7], reflecting an obvious difference between the *in vivo* and *in vitro* models or a species difference. The mechanism through which TM6SF2 deficiency might impair mitochondrial function remains subject of future study. In addition, any direct mechanistic link between deficient mitochondrial FA oxidation and enhanced *de novo* lipogenesis cannot yet be proposed. However, a similar situation was observed in hepatocytes from mice deficient in BNip3 [35]. In those cells, impaired mitochondrial β-oxidation was associated with *de novo* lipogenesis utilizing glucose-derived acetyl-CoA.

While the TAGs and CEs stored in cellular lipid droplets are the frequent response for improved lipogenesis or impaired utilization of lipids, the increased absolute quantities of cellular PCs and PEs found in the TM6SF2 knock-down cells formed an intriguing question. To obtain clues of the fate of these lipids, we carried out transmission EM, which revealed a markedly elevated volume of lysosomal compartments in the TM6SF2 knock-down cells. EM observation of TM6SF2-deficient hepatocytes or liver tissue has not been reported previously. Thus, this observation is novel. It may reflect a homeostatic response triggered in order to hydrolyze an excess of membranes that harbor the accumulating phospholipids. However, the amplification of lysosomes may equally well represent a cellular metabolic adaptation unrelated to the cellular phospholipid excess.

Together with human studies such as that of Luukkonen et al. [36] on the role of hepatic ceramides in NAFLD, our work supports a lipocentric view to liver disease. One can envision that subjects carrying variants of genes such as TM6SF2 or MBOAT7 [3,32] might benefit from dietary supplementation with PUFAs. On the other hand, preventing CVD by depressing TM6SF2 function [5] might lead to a risk of developing liver disease; therefore, such therapeutic strategies should be considered with caution.

TM6SF2 knock-down in human HuH7 hepatoma cells resulted in the enrichment of SFAs/MUFAs in several lipid classes, depletion of PCs with AA, reduced mitochondrial FA oxidation and amplification of late endosomal/lysosomal membrane compartment. Under normal conditions, a dynamic PUFA-enriched ER membrane domain allows the efficient synthesis of apoB-lipoprotein particles, and hepatocellular lipid homeostasis is maintained. Upon TM6SF2 depletion, phospholipids with SFAs and MUFAs accumulate and PUFAs are reduced, resulting in a defect of assembly of apoB lipoproteins with a normal size and lipid composition, associated with cellular neutral lipid accumulation, reduced FA oxidation and an enlarged lysosomal compartment (see Graphical Abstract). The mitochondrial FA oxidation defect could be due to (i) an unoptimal composition of the mitochondrial membranes, (ii) altered ER membrane structure decreasing the size of the secreted lipid particles and possibly impairing the FA flux to mitochondria, and finally (iii) altered structure of the ER membranes disturbing the ER-mitochondial contacts and thereby the flux of FA and also importantly the flux of Ca^{2+} between the organelles [37]. Further functional studies are warranted to distinguish between the mechanisms hypothesized above.

To conclude, the present observations provide novel clues to the function of TM6SF2 and the mechanism(s) by which the deficiency of the protein disturbs hepatic lipoprotein mediated TAG secretion. Specifically they suggest that the impaired secretion is associated with distorted dynamics of membrane phospholipid synthesis/degradation affected by the unoptimal phospholipid FA composition.

Funding

This study was supported by grants from the Instrumentarium Science Foundation (H.R.), the Finnish Foundation for Cardiovascular Research (V.M.O.), the Diabetes Research Foundation (P.A.N.H.), the Magnus Ehrnrooth Foundation (P.A.N.H., V.M.O.), and the Liv och Hälsa Foundation (V.M.O.).

Transparency Document

The Transparency document associated with this article can be found, in online version.

Acknowledgments

We gratefully acknowledge the skilled technical assistance by Eeva Jääskeläinen and Riikka Kosonen, and the help in EM image analysis of secreted lipoprotein-like particles by Amr Abou Elezz. We also thank the Electron Microscopy Unit, Institute of Biotechnology, University of Helsinki, for technical help and availability of instruments.

Appendix A. Supplementary data

Supplementary data to this article can be found online at http://dx.doi.org/10.1016/j.bbalip.2017.04.004.

References

[1] Z.M. Younossi, A.B. Koenig, D. Abdelatif, Y. Fazel, L. Henry, M. Wymer, Global epidemiology of nonalcoholic fatty liver disease-meta-analytic assessment of prevalence, incidence, and outcomes, Hepatology 64 (2016) 73–84.
[2] S. Romeo, J. Kozlitina, C. Xing, A. Pertsemlidis, D. Cox, L.A. Pennacchio,

E. Boerwinkle, J.C. Cohen, H.H. Hobbs, Genetic variation in PNPLA3 confers susceptibility to nonalcoholic fatty liver disease, Nat. Genet. 40 (2008) 1461–1465.
[3] J. Kozlitina, E. Smagris, S. Stender, B.G. Nordestgaard, H.H. Zhou, A. Tybjaerg-Hansen, T.F. Vogt, H.H. Hobbs, J.C. Cohen, Exome-wide association study identifies a TM6SF2 variant that confers susceptibility to nonalcoholic fatty liver disease, Nat. Genet. 46 (2014) 352–356.
[4] R.M. Mancina, P. Dongiovanni, S. Petta, P. Pingitore, M. Meroni, R. Rametta, J. Borén, T. Montalcini, A. Pujia, O. Wiklund, G. Hindy, R. Spagnuolo, B.M. Motta, R.M. Pipitone, A. Craxi, S. Fargion, V. Nobili, P. Käkelä, V. Kärjä, V. Männistö, J. Pihlajamäki, D.F. Reilly, J. Castro-Perez, J. Kozlitina, L. Valenti, S. Romeo, The MBOAT7-TMC4 variant rs641738 increases risk of nonalcoholic fatty liver disease in individuals of European descent, Gastroenterology 150 (2016) (1219-1230.e6).
[5] O.L. Holmen, H. Zhang, Y. Fan, D.H. Hovelson, E.M. Schmidt, W. Zhou, Y. Guo, J. Zhang, A. Langhammer, M.L. Lochen, S.K. Ganesh, L. Vatten, F. Skorpen, H. Dalen, J. Zhang, S. Pennathur, J. Chen, C. Platou, E.B. Mathiesen, T. Wilsgaard, I. Njolstad, M. Boehnke, Y.E. Chen, G.R. Abecasis, K. Hveem, C.J. Willer, Systematic evaluation of coding variation identifies a candidate causal variant in TM6SF2 influencing total cholesterol and myocardial infarction risk, Nat. Genet. 46 (2014) 345–351.
[6] Y. Fan, H. Lu, Y. Guo, T. Zhu, M.T. Garcia-Barrio, Z. Jiang, C.J. Willer, J. Zhang, Y.E. Chen, Hepatic transmembrane 6 superfamily member 2 regulates cholesterol metabolism in mice, Gastroenterology 150 (2016) 1208–1218.
[7] E. Smagris, S. Gilyard, S. BasuRay, J.C. Cohen, H.H. Hobbs, Inactivation of Tm6sf2, a Gene defective in fatty liver disease, impairs Lipidation but not secretion of very low density lipoproteins, J. Biol. Chem. 291 (2016) 10659–10676.
[8] H. Mahdessian, A. Taxiarchis, S. Popov, A. Silveira, A. Franco-Cereceda, A. Hamsten, P. Eriksson, F. van't Hooft, TM6SF2 is a regulator of liver fat metabolism influencing triglyceride secretion and hepatic lipid droplet content, Proc. Natl. Acad. Sci. U. S. A. 111 (2014) 8913–8918.
[9] T. Hashidate-Yoshida, T. Harayama, D. Hishikawa, R. Morimoto, F. Hamano, S.M. Tokuoka, M. Eto, M. Tamura-Nakano, R. Yanobu-Takanashi, Y. Mukumoto, H. Kiyonari, T. Okamura, Y. Kita, H. Shindou, T. Shimizu, Fatty acid remodeling by LPCAT3 enriches arachidonate in phospholipid membranes and regulates triglyceride transport, elife 4 (2015), http://dx.doi.org/10.7554/eLife.06328.
[10] J. Folch, M. Lees, G.H. Sloane Stanley, A simple method for the isolation and purification of total lipides from animal tissues, J. Biol. Chem. 226 (1957) 497–509.
[11] K.L. Duffin, J.D. Henion, J.J. Shieh, Electrospray and tandem mass spectrometric characterization of acylglycerol mixtures that are dissolved in nonpolar solvents, Anal. Chem. 63 (1991) 1781–1788.
[12] K. Duffin, M. Obukowicz, A. Raz, J.J. Shieh, Electrospray/tandem mass spectrometry for quantitative analysis of lipid remodeling in essential fatty acid deficient mice, Anal. Biochem. 279 (2000) 179–188.
[13] B. Brügger, G. Erben, R. Sandhoff, F.T. Wieland, W.D. Lehmann, Quantitative analysis of biological membrane lipids at the low picomole level by nano-electrospray ionization tandem mass spectrometry, Proc. Natl. Acad. Sci. U. S. A. 94 (1997) 2339–2344.
[14] P. Haimi, A. Uphoff, M. Hermansson, P. Somerharju, Software tools for analysis of mass spectrometric lipidome data, Anal. Chem. 78 (2006) 8324–8331.
[15] R. Käkelä, A. Käkelä, S. Kahle, B.H. Becker, A. Kelly, R.W. Furness, Fatty acid signatures in plasma of captive herring gulls as indicators of demersal or pelagic fish diet, Mar. Ecol. Prog. Ser. 293 (2005) 191–200.
[16] E.G. Bligh, W.J. Dyer, A rapid method of total lipid extraction and purification, Can. J. Biochem. Physiol. 37 (1959) 911–917.
[17] P. Ylä-Anttila, H. Vihinen, E. Jokitalo, E.L. Eskelinen, Monitoring autophagy by electron microscopy in mammalian cells, Methods Enzymol. 452 (2009) 143–164.
[18] S. Wold, M. Sjöström, SIMCA: a method for analyzing chemical data in terms of similarity and analogy, in: B. Kowalski (Ed.), Chemometrics: Theory and Application, American Chemical Society, Washington D.C., 1977, pp. 243–282.
[19] P. Dongiovanni, S. Petta, C. Maglio, A.L. Fracanzani, R. Pipitone, E. Mozzi, B.M. Motta, D. Kaminska, R. Rametta, S. Grimaudo, S. Pelusi, T. Montalcini, A. Alisi, M. Maggioni, V. Kärjä, J. Borén, P. Käkelä, V. Di Marco, C. Xing, V. Nobili, B. Dallapiccola, A. Craxi, J. Pihlajamäki, S. Fargion, L. Sjöström, L.M. Carlsson, S. Romeo, L. Valenti, Transmembrane 6 superfamily member 2 gene variant disentangles nonalcoholic steatohepatitis from cardiovascular disease, Hepatology 61 (2015) 506–514.
[20] H. Malhi, S.F. Bronk, N.W. Werneburg, G.J. Gores, Free fatty acids induce JNK-dependent hepatocyte lipoapoptosis, J. Biol. Chem. 281 (2006) 12093–12101.
[21] A. Kotronen, T. Seppänen-Laakso, J. Westerbacka, T. Kiviluoto, J. Arola, A.L. Ruskeepää, M. Oresic, H. Yki-Järvinen, Hepatic stearoyl-CoA desaturase (SCD)-1 activity and diacylglycerol but not ceramide concentrations are increased in the nonalcoholic human fatty liver, Diabetes 58 (2009) 203–208.
[22] F. Xiao, J. Deng, Y. Guo, Y. Niu, F. Yuan, J. Yu, S. Chen, F. Guo, BTG1 ameliorates liver steatosis by decreasing stearoyl-CoA desaturase 1 (SCD1) abundance and altering hepatic lipid metabolism, Sci. Signal. 9 (2016) ra50.
[23] Z.Z. Li, M. Berk, T.M. McIntyre, A.E. Feldstein, Hepatic lipid partitioning and liver damage in nonalcoholic fatty liver disease: role of stearoyl-CoA desaturase, J. Biol. Chem. 284 (2009) 5637–5644.
[24] B.M. Arendt, E.M. Comelli, D.W. Ma, W. Lou, A. Teterina, T. Kim, S.K. Fung, D.K. Wong, I. McGilvray, S.E. Fischer, J.P. Allard, Altered hepatic gene expression in nonalcoholic fatty liver disease is associated with lower hepatic n-3 and n-6 polyunsaturated fatty acids, Hepatology 61 (2015) 1565–1578.
[25] L. Wang, S. Athinarayanan, G. Jiang, N. Chalasani, M. Zhang, W. Liu, Fatty acid desaturase 1 gene polymorphisms control human hepatic lipid composition, Hepatology 61 (2015) 119–128.
[26] X. Rong, B. Wang, M.M. Dunham, P.N. Hedde, J.S. Wong, E. Gratton, S.G. Young, D.A. Ford, P. Tontonoz, Lpcat3-dependent production of arachidonoyl phospholipids is a key determinant of triglyceride secretion, elife 4 (2015), http://dx.doi.org/10.7554/eLife.06557.
[27] G.S. Shelness, J.A. Sellers, Very-low-density lipoprotein assembly and secretion, Curr. Opin. Lipidol. 12 (2001) 151–157.
[28] S.A. Siddiqi, VLDL exits from the endoplasmic reticulum in a specialized vesicle, the VLDL transport vesicle, in rat primary hepatocytes, Biochem. J. 413 (2008) 333–342.
[29] E.A. O'Hare, R. Yang, L.M. Yerges-Armstrong, U. Sreenivasan, R. McFarland, C.C. Leitch, M.H. Wilson, S. Narina, A. Gorden, K.A. Ryan, A.R. Shuldiner, S.A. Farber, G.C. Wood, C.D. Still, G.S. Gerhard, J.D. Robishaw, C. Sztalryd, N.A. Zaghloul, TM6SF2 rs58542926 impacts lipid processing in liver and small intestine, Hepatology (2017), http://dx.doi.org/10.1002/hep.29021 (Epub ahead of print).
[30] J.S. Lee, R. Mendez, H.H. Heng, Z.Q. Yang, K. Zhang, Pharmacological ER stress promotes hepatic lipogenesis and lipid droplet formation, Am. J. Transl. Res. 4 (2012) 102–113.
[31] H. Ruhanen, J. Perttilä, M. Hölttä-Vuori, Y. Zhou, H. Yki-Järvinen, E. Ikonen, R. Käkelä, V.M. Olkkonen, PNPLA3 mediates hepatocyte triacylglycerol remodeling, J. Lipid Res. 55 (2014) 739–746.
[32] P.K. Luukkonen, Y. Zhou, T. Hyötyläinen, M. Leivonen, J. Arola, M. Orho-Melander, M. Orešič, H. Yki-Järvinen, The MBOAT7 variant rs641738 alters hepatic phosphatidylinositols and increases severity of non-alcoholic fatty liver disease in humans, J. Hepatol. 65 (2016) 1263–1265.
[33] S.H. Caldwell, R.H. Swerdlow, E.M. Khan, J.C. Iezzoni, E.E. Hespenheide, J.K. Parks, W.D. Parker Jr., Mitochondrial abnormalities in non-alcoholic steatohepatitis, J. Hepatol. 31 (1999) 430–434.
[34] J.A. Ibdah, P. Perlegas, Y. Zhao, J. Angdisen, H. Borgerink, M.K. Shadoan, J.D. Wagner, D. Matern, P. Rinaldo, J.M. Cline, Mice heterozygous for a defect in mitochondrial trifunctional protein develop hepatic steatosis and insulin resistance, Gastroenterology 128 (2005) 1381–1390.
[35] D. Glick, W. Zhang, M. Beaton, G. Marsboom, M. Gruber, M.C. Simon, J. Hart, G.W. Dorn II, M.J. Brady, K.F. Macleod, BNip3 regulates mitochondrial function and lipid metabolism in the liver, Mol. Cell. Biol. 32 (2012) 2570–2584.
[36] P.K. Luukkonen, Y. Zhou, S. Sädevirta, M. Leivonen, J. Arola, M. Orešič, T. Hyötyläinen, H. Yki-Järvinen, Hepatic ceramides dissociate steatosis and insulin resistance in patients with non-alcoholic fatty liver disease, J. Hepatol. 64 (2016) 1167–1175.
[37] G. Csordás, P. Várnai, T. Golenár, S. Roy, G. Purkins, T.G. Schneider, T. Balla, G. Hajnóczky, Imaging interorganelle contacts and local calcium dynamics at the ER-mitochondrial interface, Mol. Cell 39 (2010) 121–132.